Int J Adv Manuf Technol (2002) 20:397–406

The International Journal of
Advanced Manufacturing Technology

Energy Dissipation Control in Hydro-Abrasive Machining Using Quantitative Acoustic Emission

R. S. Mohan[1], A. W. Momber[2] and R. Kovacevic[3]

[1]Department of Mechanical Engineering, The University of Tulsa, Tulsa, Oklahoma, USA; [2]WOMA Apparatebau GmbH, Duisburg, Germany; and [3]Department of Mechanical Engineering, Southern Methodist University, Dallas, Texas, USA

The efficiency and product quality of hydro-abrasive machining (HAM) could be considerably improved if the energy dissipation phenomenon of the jet-like tool during the material removal is clearly understood. An on-line technique for quantifying the amount of energy dissipated in the workpiece during HAM using acoustic emission (AE) measurements is presented in this paper. The measured AE-signals are linked to a physical energy dissipation model. Stochastic modelling of the AE-signals provides more information on the physics of the energy dissipation process.

Keywords: Acoustic emission; Energy dissipation; Hydro-abrasive machining

1. Introduction

Acoustic emission (AE) refers to stress waves or elastic waves produced by a sudden release of energy during microscopic deformations or fracture occurring in materials as they are stressed. The AE-sensing technique has been used as a tool for monitoring different phenomena associated with manufacturing processes such as tool wear [1,2], tool breakage [3,4], non-destructive evaluation [5,6] and surface roughness [4,7]. Even though AE-sensing has proved to be suitable for application in monitoring traditional manufacturing processes such as turning [3,4], milling [1], drilling [8,9], grinding [2,10–13], micromachining [14], its use for modern manufacturing processes such as hydro-abrasive machining (HAM) has been limited. Owing to their capability of sensing the sudden release of energy in materials, AE-signals offer the potential to monitor energy dissipation phenomena during the material removal processes. A review of the applications of AE-sensing technique in abrasive wear, erosion, fracture, and related mechanisms is given in Table 1. Table 2 gives several attempts that were made to use the AE-technique for monitoring certain process features of HAM.

Nowadays, HAM is being used increasingly for machining difficult-to-machine materials such as glass, ceramics [22,25], cementitious composites [24], fibre-reinforced composite materials [27], and titanium [28], owing to its versatility as an effective machining technique. As a manufacturing tool, if properly controlled, HAM has good potential for 3D machining of materials [29]. An example is shown in Fig. 1. Also called abrasive injection jet, the jet-like tool is formed by accelerating abrasive particles (garnet, aluminium oxide or silicon carbide) of typically 400 μm diameter by a high-speed waterjet as it flows through a focusing tube. A large number of abrasive particles (about 10^5 s^{-1}) are entrained in the two-phase mixture (water and air) and exit from the mixing nozzle at speeds of several hundred metres per second. Process parameters such as pump pressure, orifice diameter, nozzle diameter, traverse rate, abrasive flowrate, abrasive material and size, stand-off distance, and mixing chamber geometry [29] influence the performance of the process jointly and independently.

Energy conversion analysis indicates that in HAM only a part of the input energy is consumed for useful work in the material removal process. A considerable portion of the input energy is carried away by the exiting mixture of abrasives, water and wear particles [30,31]. The remaining energy is dissipated by related mechanisms, such as wall friction, heat formation, plastic deformation, and water and solid film damping. These mechanisms are discussed in detail in a related paper [32]. The machining performance in terms of material removal rate, erosion depth and surface finish is influenced considerably by the energy dissipated in the workpiece. Studies performed by Nadeau et al. [33] indicate that the material removal rate, and hence the erosion depth, is directly proportional to the kinetic energy of the abrasive particles. Preliminary investigations of Zhou et al. [34], followed by a detailed study by Raju and Ramulu [35], suggest that the available local kinetic energy of the abrasive particles determines the quality of the cut at various regions. Thus, it can be seen that the energy dissipated in the workpiece during the material removal process is a good indictor of the process performance

Correspondence and offprint requests to: Dr-Ing. A. Momber, WOMA Apparatebau GmbH, Postfach 14 18 20, 47208 Duisberg, Germany. E-mail: andreas.momber@woma.de

Table 1. Relationship between material removal mechanism, energy dissipation phenomena, and AE-signal parameter.

Removal mechanism	Related process parameter	AE-parameter	Reference
Cavitating jet	Depth of deformation	AE-energy	Okamura et al. [15]
Cavitation	Cavitation energy level	r.m.s.-voltage	Derakhshan et al. [6]
Indentation fracture	Chip formation energy	r.m.s.-voltage	Jung et al. [8]
Abrasion wear	Material removal power	r.m.s.-voltage	Matsuoka et al. [16]
Sliding wear	Frictional work Deformed volume	AE-counts AE-energy	Lingard and Ng [17] Lingard et al. [18]
Lubricated sliding wear	Wear volume	r.m.s.-voltage	Bones and McBride [5]
Sliding contact	Frictional energy	r.m.s.-voltage	Jiaa and Dornfeld [19]
Contact damage	Micro-fracture damage	AE-energy	Guiberteau et al. [20]
Water jet erosion	Erosion mode	r.m.s.-voltage	Momber [21]

Table 2. Use of AE-technique to monitor process features of HAM.

Material	AE-parameters	HAM feature	Reference
Alumina ceramics	r.m.s.-voltage	Borehole cracking	Choi and Choi [22]
Aluminium	PSD (ARMA-modelling) Amplitude	Erosion depth Cutting-through control	Mohan et al. [23]
Concrete	FFT-peak, frequency and amplitude	Macroscopic material removal Material property influence	Momber et al. [24]
Refractory ceramics	Signal amplitude	Material fracture mode	Momber et al. [25]
	Signal amplitude PSD (ARMA-modelling)	Individual piercing stages Hole quality	Kovacevic et al. [26]

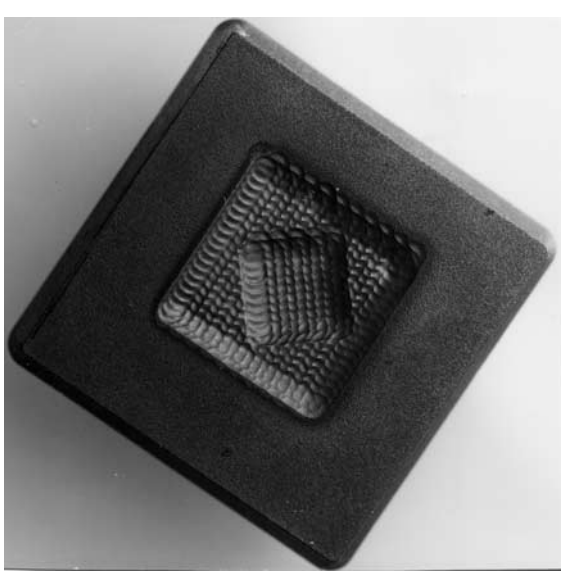

Fig. 1. 3D-pocket milling of a steel sample by HAM; size: Matchbox (Photograph: Chalmers University of Technology, Göteborg, Sweden).

in terms of quality and efficiency. However, no physical model has been suggested nor has any parameter yet been identified that are capable of determining the energy dissipated during HAM.

This investigation attempts to develop a simple physical model for calculating the energy dissipated during HAM. The feasibility of monitoring this energy on-line during the erosion process using an AE-sensing technique is also investigated. The power spectrum density (PSD) of the autoregressive moving average (ARMA) model, representing the AE-signal, is checked as a potential parameter. Moreover, the potential of the area enclosed by the PSD-curve to measure quantitatively the dissipated energy is investigated. It is also investigated whether the frequency decomposition of the ARMA-models provides more insight into the energy dissipation during HAM.

2. Energy Dissipation Model

A simple physical model is derived from first principles to estimate the energy dissipated in the workpiece during the material removal by HAM. The kinetic energy, E_A, of a high-speed abrasive–water flow is given by:

$$E_A = 0.5\, m_A\, v_A^2 \tag{1}$$

Here, m_A is the mass of the abrasive–water mixture, and v_A is the velocity of the mixture. The mass of the abrasive–water mixture is given by:

$$m_A = (\dot{m}_P + \dot{m}_W)t_E \tag{2}$$

In this equation, $\dot{m}_P$ is the mass flowrate of the abrasive, $\dot{m}_W$ is the mass flowrate of the water, and t_E is the exposure time given by:

$$t = \frac{d_F}{v} \tag{3}$$

Here, d_F is the diameter of the mixing nozzle, and v is the traverse rate of the machining head.

Assuming a simple momentum transfer between the high-speed water flow and the incoming solid particles in the mixing chamber, and neglecting the air mass flowrate, the velocity of the abrasive water mixture can be expressed by:

$$v_A = \alpha \frac{v_W}{1 + (\dot{m}_P/\dot{m}_W)} \tag{4}$$

Here, α is a mixing efficiency coefficient, and v_W is the velocity of the water flow entering the mixing nozzle. It may be noted that α can be estimated very effectively by impact force measurement [36]. The velocity of the high-speed water flow can be calculated using Bernoulli's principles which yields:

$$v_W = \varphi \sqrt{\left(\frac{2p}{\rho_W}\right)} \tag{5}$$

Here, p is the applied pump pressure, ρ_W is the density of water, and φ is the orifice momentum transfer coefficient which can be estimated, for example, by impact force measurements [36]. Substituting Eqs (2)–(5) into (1) leads to:

$$E_A = \frac{\alpha^2 \varphi^2 d_F p(\dot{m}_P + \dot{m}_W)}{v\rho_W (1 + (\dot{m}_P/\dot{m}_W))^2} \tag{6}$$

Equation (6) gives the input energy to the HAM-process. Part of this input energy, E_{DISS}, is dissipated in the workpiece through various mechanisms, such as material fracture, friction, and damping. The rest, E_{EX}, is carried by the exiting slurry after erosion. The diagram of the energy dissipation during HAM is shown in Fig. 2. A simple energy balance gives:

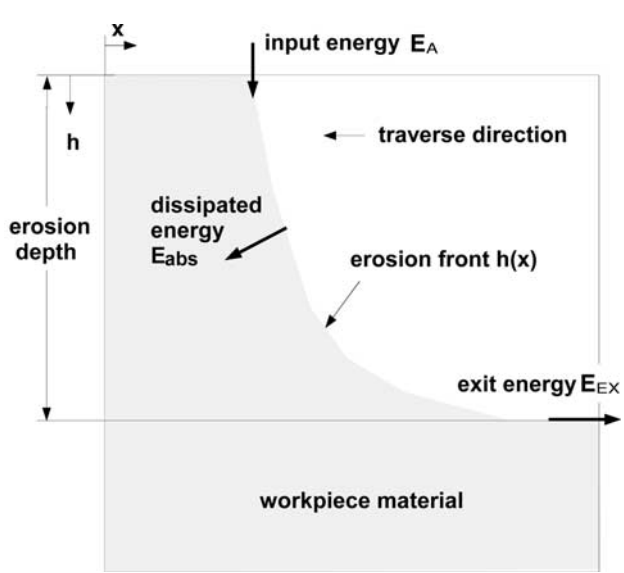

Fig. 2. Energy dissipation in a workpiece during HAM.

$$E_A = E_{DISS} + E_{EX} \tag{7}$$

A mathematical model for the calculation of the exit energy of the abrasive–water mixture for erosive separation is developed by Momber and Kovacevic [30]. However, for kerfing operations a different approach must be adopted for calculating the exit energy. Experimental results [29,37] have indicated that the material removal process in HAM is initiated when the pump pressure exceeds a critical pressure known as the threshold pressure, p_T. The threshold pressure for each material can be estimated experimentally from the plot of erosion depth versus applied pump pressure [29]. It can also be assumed that in pocket erosion, as the abrasive–water mixture leaves the workpiece under the critical condition that it is unable to remove more material, the critical pressure represents the exit energy of this mixture. Incorporating these assumptions in Eqs (6) and (7) yields:

$$E_{DISS} = \frac{\alpha^2 \varphi^2 d_F (\dot{m}_P + \dot{m}_W)}{v\rho_W \left(1 + \frac{\dot{m}_P}{m_W}\right)^2} [p - p_T] \tag{8}$$

Thus, Eq. (8) can be used to calculate the amount of energy dissipated during the HAM by different mechanisms, such as plastic deformation, material fracture, wall friction, cavitation, turbulent vortices, and film damping. It may be noted that the parameters in Eq. (8) are either known or could be measured, and that the variables, α, φ, and p_T depend on other process parameters.

In HAM, the AE-signals are generated primarily by material failure due to cracking, micromachining, erosion etc., as well as to turbulent vortices, cavitation, and the interaction of droplets and abrasive particles with the material, caused by the flow of the abrasive–water mixture [23]. As the energy dissipated during the machining process is responsible for the above phenomena, it is intuitive to expect that the AE-signal will be capable of quantifying the energy dissipation events in the workpiece during HAM.

In order to measure the energy of the AE-signal, the time-domain signal is modelled using a suitable ARMA-model. The power spectrum density (PSD) of the model is determined, and the area under the PSD-curve gives the energy of the AE-signal which is a measure of the dissipated energy in HAM. The results obtained from Eq. (8) are used to investigate the feasibility of monitoring the energy dissipated in the workpiece using the AE-sensing technique.

3. Experimental Set-Up and Procedure

The experimental set-up shown in Fig. 3 consists of an HAM-system, AE-sensor, pre-amplifier, A/D-converter, AE-monitoring system, and PC/AT with suitable software and the workpiece. The HAM-system used for conducting the experiment consists of a high-pressure intensifier pump, machining head, abrasive metering and delivery system, abrasive hopper with garnet as the abrasive, catcher tank, and *X-Y-Z* positioning system controlled by a CNC-controller.

The generated AE-signals were detected and processed by a Model AET 5500 Acoustic Emission Monitoring System which

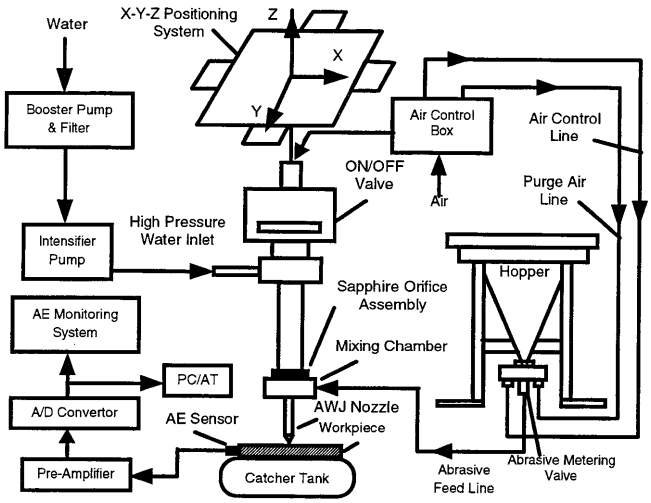

Fig. 3. Experimental set-up.

consists of an AET 5500 mainframe (signal processing unit), graphics terminal (interface, data storage and display) and accessories (sensors, pre-amplifiers etc.). When an acoustic emission, caused by an induced stress, occurs in a test specimen, the sensors (resonant frequency = 2 MHz), fixed on the side walls of the specimens, convert this acoustic wave into a voltage signal which is amplified by the pre-amplifier and sent to the mainframe (16-bit microprocessor) for post-processing. The distance between the erosion site and sensor was about 20 mm. The sensor was fixed on the samples with a water resistant epoxy-resin. The workpiece used for investigation was grey cast iron of 51 mm thickness (see Table 3).

The HAM-process parameters, namely water pressure and traverse speed, were varied and linear kerfs were eroded on the workpiece. The raw signal from the AE-monitoring system was acquired using a suitable PC-based data acquisition system for stochastic modelling and spectrum analysis. The respective erosion depths were also measured. The process parameters for these experiments are given in Table 3.

Table 3. Experimental parameters.

Hydro-abrasive machining	
Abrasive material	Garnet
Abrasive mesh size	# 36
Abrasive particle shape	Angular (random)
Abrasive mass flow rate	0.30 kg min^{-1}
Orifice material	Sapphire
Orifice diameter	0.457 mm
Mixing nozzle length	88.9 mm
Mixing nozzle diameter	1.27 mm
Stand-off distance	6.00 mm
Method of feed	Suction
Abrasive condition	Dry
Impact angle	90°
Workpiece details	
Material	Grey cast iron (ASTM grade 40)
Material thickness	51 mm
Erosion track length	100 mm
Experimental variables	
Range of operating pressure	90–241 MPa
Range of traverse rate	0.42–3.39 mm s^{-1}

In order to study the frequency response characteristics of acoustic emission, the raw signal was acquired at different frequencies, namely f_A = 500 kHz, 1 MHz, and 2 MHz. The time domain signal consisting of 5120 observations is modelled using the ARMA-modelling technique. An ARMA (m, n) model can be represented by the equation,

$$Y_t - \Phi_1 Y_{t-1} - \Phi_2 Y_{t-2} - \ldots - \Phi_m Y_{t-m} = \Theta_1 a_{t-1} - \Theta_2 a_{t-2} - \ldots \Theta_n a_{t-n} \quad (9)$$

Here, Y_t is the amplitude of the signal at time t, a_t is the noise, and $a_t \cong \mathrm{NID}(0,\sigma_a^2)$. The best fit ARMA-model [ARMA (4,3)] is determined by analysing the variance of a_t using the F-criterion. The power spectrum density function of the ARMA (m, n) model is given by the following Eq. [38]:

$$P(f) = 2\sigma_a^2 \quad (10)$$

$$\frac{\left|1 - \Theta_1 e^{-i2\pi f} - \Theta_2 e^{-4\pi f} - \ldots - \Theta_n e^{-i2\pi nf}\right|^2}{\gamma_0 \left|1 - \Phi_1 e^{-i2\pi f} - \Phi_2 e^{-i4\pi f} - \ldots - \Phi_m e^{-i2\pi mf}\right|^2}$$

Here,

$$0 \le f \le \tfrac{1}{2},\ \gamma_0 = \sum_{i=1}^{m} d_i, \text{ and } d_i = \sum_{j=1}^{m} \frac{g_i g_j}{1 - \lambda_i \lambda_j}$$

The λ terms are the characteristic roots of the ARMA-model, and g_i is given by:

$$g_i = \frac{(\lambda_i^n - \Theta_1 \lambda_i^{n-1} - \ldots - \Theta_n)}{(\lambda_i - \lambda_1)(\lambda_i - \lambda_2) \ldots (\lambda_i - \lambda_{i-1})(\lambda_i - \lambda_{i+1}) \ldots (\lambda_i - \lambda_m)} \quad (11)$$

The power spectrum density of the best-fit ARMA-model is obtained for further analysis.

4. Results and Discussion

4.1 Results of the Physical Energy Dissipation Model

The results of the energy calculations using the physical model proposed in Eq. (8) are shown in Fig. 4. The energy dissipated in the workpiece is 60%–90% of the HAM input energy. These values depend on the erosion depth and on the input energy, respectively. For lower energies and lower depths, the relative amount of dissipated energy is lower. This trend is in general agreement with wear-debris size measurements during the HAM of cast iron carried out by Momber et al. [37] who found a drop in the material removal efficiency for high pump pressures. Momber and Kovacevic [32] observed a decrease in the efficiency of concrete erosion by HAM with increasing pressure as well as decreasing traverse rate. It can be seen in Fig. 4 that there is a significant relationship between the erosion depth and the energy dissipated during the erosion. This relationship can be fitted very reasonably by a second-order polynomial (R^2 = 0.94):

$$E_{DISS} = C_1 h^2 + C_2 h + C_3 \quad (C_3 = 0) \quad (12)$$

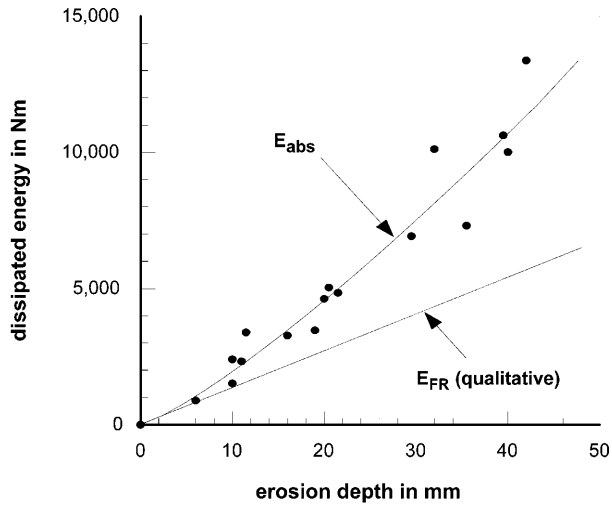

Fig. 4. Relationship between erosion depth and calculated dissipated energy according to Eq. (8).

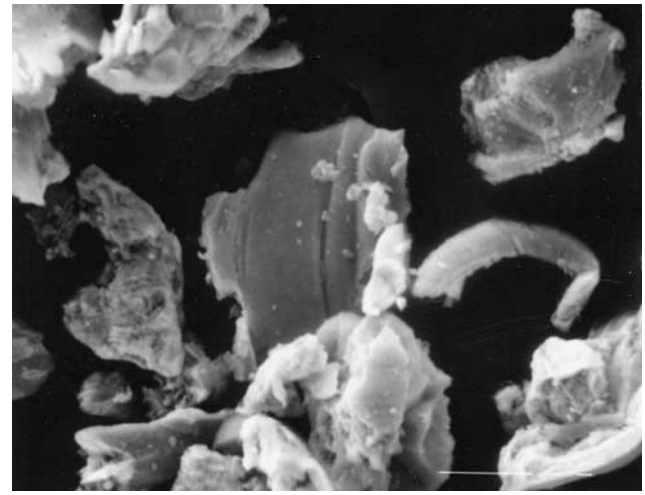

Fig. 5. SEM-photograph of grey cast iron wear debris, generated during HAM (scale: 100 μm); Parameters: p=138 MPa, $\dot{m}_P$ = 4.3 g s^{-1}, abrasive: garnet #36).

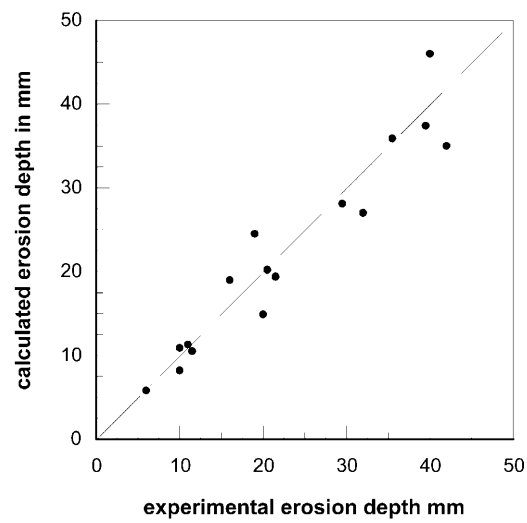

Fig. 6. Calculated erosion depth based on Zeng and Kim's [42] model and experimental results.

This type of approximation was also found by Momber and Kovacevic [31] for the relationship between the erosion depth and a relative energy dissipation coefficient for aluminium, steel, and cast iron. The relative energy dissipation coefficient is a parameter estimated from the geometry of the erosion front. A second-order polynomial was also successfully used by Chao and Geskin [39] to relate the peak amplitude of the striations generated by HAM and the erosion depth. Finally, Tan's model [40] for the surface waviness height in HAM gives a second-order polynomial between the erosion depth and the average waviness. These similarities support the general solution obtained from the physical energy dissipation model.

The nonlinear progress of the function plotted in Fig. 4 suggests the action of different energy dissipation mechanisms during HAM. With regard to material failure, grey cast iron is assumed to behave as a brittle material. In grey cast iron, the graphite flakes, which could be considered essentially as sharp cracks, inhibit deformation of the normally ductile ferrite and produce a very brittle behaviour. This has been observed by Momber et al. [41] during HAM of grey cast iron. However, removed erosion debris sometimes shows features of plastic deformation and microcutting, as illustrated in Fig. 5. Therefore, the formation of debris may be assumed to be a process of crack-network generation and ductile plastic deformation, as supposed by Zeng and Kim [42] in a model for HAM of brittle materials. This assumption is supported by Fig. 6 which shows a comparative plot of values based on this model and experimentally estimated erosion depths. Except for two larger deviations, the model fits very well. Zeng and Kim's [42] model states a relationship between the erosion resistance, R_E, and the specific surface energy of a material, γ_M, which is given by:

$$R_E \propto \gamma_M \tag{13}$$

The energy which is dissipated during the generation of erosion debris may be:

$$E_{FR} = (\gamma_M + \gamma_{PL})\, 2S_P \tag{14}$$

Here, S_P is the surface area of the wear debris sample, and γ_{PL} characterises mechanisms of plastic deformation and toughening in the material, that may operate even in brittle-behaving materials as they are subjected to very high-impact velocities at a microscopic scale. Direct measurements of the surfaces of HAM-generated cast iron wear particles [37] have shown the following:

$$S_P = a_1\, h \tag{15}$$

Here, h is the erosion depth. Therefore,

$$E_{FR} = 2a_1(\gamma_M + \gamma_{PL})\, h \propto h$$
$$a_1 = \text{constant} \tag{16}$$

Equation (16) suggests a linear relationship between the erosion depth and the energy dissipated in wear debris formation. For better understanding, this function is qualitatively plotted in

Fig. 4. A typical value for E_{FR} is about 2% of the kinetic input energy [32,37]. The increasing discrepancy between E_{DISS} and E_{FR} with increasing erosion depth may be because additional dissipation mechanisms, such as fluid film damping, wall friction, and turbulence, become important with increasing depth [32]. This conclusion follows the logic of the HAM process and may explain the rising progress of the energy dissipation function with increasing erosion depth.

4.2 Frequency Response Characteristics of Acoustic Emission

AE-measurement performed by Tikhomirov et al. [43] during HAM of reinforced plastics indicated that the AE-signals generated by the abrasive–water flow have frequencies between $f_A = 100$ and $f_A = 600$ kHz, whereas those generated by material failure were noticed at frequencies between $f_A = 750$ kHz and $f_A = 1200$ kHz. In order to study the frequency response characteristics of AE-signals generated during the HAM of grey cast iron, preliminary investigations were conducted by acquiring signals at $f_A = 500$ kHz, 1 MHz, and 2 MHz sampling frequencies. A typical time domain signal acquired at $f_A = 2$ MHz sampling frequency is shown in Fig. 7(*a*). Figures 7(*b*) to 7(*d*) show the frequency-domain AE-signals (averaged over 5 data sets) generated in the cast iron workpiece for different parameter settings. It can be seen that the energy of the signal is spread over the frequency range of 100–500 kHz. At higher water pressures (Fig. 7(*b*)), the peak frequency of the signal is concentrated around 150 kHz. With a decrease in water pressure, the response of the signal is spread over a wider frequency range. This aspect is discussed in detail in later sections.

As the frequency response is flat beyond a frequency of 500 kHz, the AE-signals acquired at a sampling frequency of $^1\lceil f_A = 1$ MHz were used for stochastic modelling. With the increase in erosion depth, the energy dissipated by the workpiece increases (see Fig. 4). Hence, the amplitude of the AE-signal can also be expected to increase. This trend is not quite evident from the fast Fourier transform (FFT) plots shown in Figs 7(*a*) to 7(*d*), which could be due to the presence of white noise. The PSD, being the Fourier cosine transform of the auto covariance function, can be expected to exhibit a trend similar to that of the FFT-curve. However, the PSD will be much smoother than a simple FFT, as it is derived from the ARMA-model which represents the trend of the signal devoid of white noise.

4.3 Behaviour of AE-Signals with Energy Dissipation

The best-fit ARMA-models obtained from the time domain AE-signals are listed in Table 4. The PSDs of the ARMA-models for various process parameters are plotted in Fig. 8. It can be seen that the PSD-curve is capable of revealing the trends properly. Any parameter change (pressure or traverse rate) which tends to increase the energy dissipated during machining causes an upward shift in the PSD-curve. Note the different scales used for the ordinate in Figs 8(*a*) to 8(*c*).

The hydrodynamic effects of the abrasive–water mixture in the erosion region change as the energy dissipated changes. The cavitation caused by the highly turbulent flow in the eroded kerf [44] leads to cavitation pressure pulses which can be reliably measured using the AE-sensing technique [6]. As noted earlier, in HAM an AE-signal is also generated by the impact of the abrasive particles and water droplets on the workpiece material, and because of material failure caused by cracking, micro-machining, etc. At higher water pressures, the cuts produced are deeper and the power spectrum density is

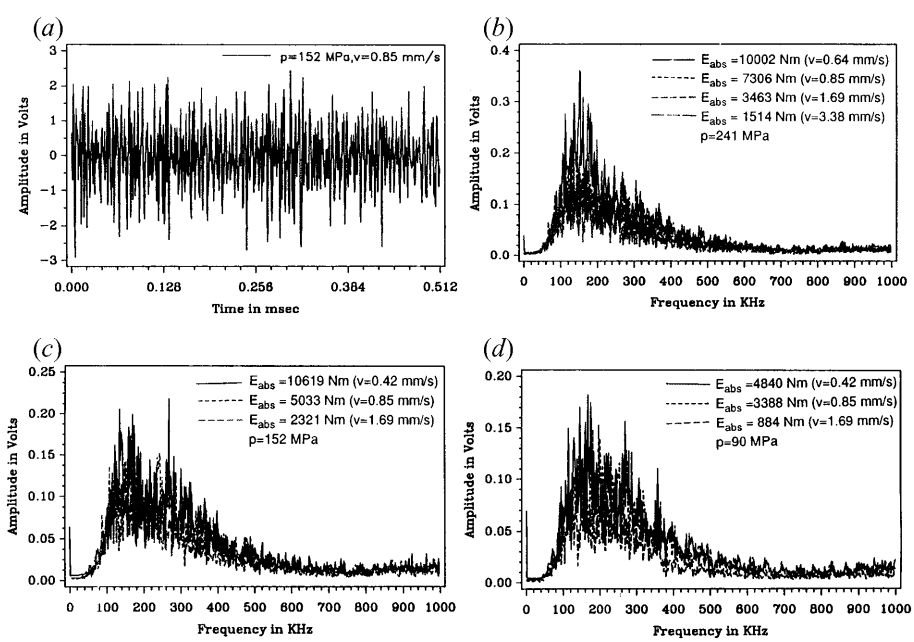

Fig. 7. Typical AE-signals for different erosion conditions. (*a*) Time-domain signal for $p = 152$ MPa. (*b*) FFT-plot for $p = 241$ MPa. (*c*) FFT-plot for $p = 152$ MPa. (*d*) FFT-plot for $p = 90$ MPa.

Table 4. Parameters of the ARMA-modelling.

Pressure (MPa)	Traverse rate (mm s^{-1})		ARMA models	σ_a	Depth (mm)	Frequency (MHz)	Damping ratio, ζ	Relative power (%)
90	1.69	Φ's →	1.0990, −0.8397, 0.3279, −0.2574	0.3574	6.0	0.275	0.297	66
		Θ's →	1.0320, −0.0184, −0.1907			0.113	0.233	34
241	3.38	Φ's →	1.2150, −0.7012, 0.0536, −0.0280	0.5504	10.0	0.249	1.008	44
		Θ's →	1.0080, 0.2305, −0.3624			0.115	0.292	56
152	1.69	Φ's →	1.5270, −1.3560, 0.5805, −0.2274	0.5493	11.0	0.215	0.430	64
		Θ's →	1.5290, −0.7441, 0.0992			0.115	0.222	36
90	0.85	Φ's →	1.2160, −1.1090, 0.4796, −0.2525	0.5900	11.5	0.243	0.316	78
		Θ's →	1.3480, −0.5458, 0.0242			0.124	0.265	22
241	1.69	Φ's →	1.3370, −1.1420, 0.5280, −0.2718	0.6559	19.0	0.245	0.310	70
		Θ's →	1.2710, −0.3396, −0.0652			0.110	0.253	30
152	0.85	Φ's →	1.3490, −1.0760, 0.4399, −0.2149	0.6888	20.5	0.242	0.385	90
		Θ's →	1.4960, −0.6145, −0.0530			0.109	0.268	10
90	0.42	Φ's →	1.0510, −0.8917, 0.3023, −0.2281	0.6886	21.5	0.266	0.334	60
		Θ's →	1.0680, −0.2272, −0.0594			0.127	0.227	40
241	0.85	Φ's →	0.9078, −0.3250, −0.1768, −0.0189	0.7310	35.5	0.441	0.646	48
		Θ's →	0.9047, 0.3461, −0.3734			0.117	0.265	52
152	0.42	Φ's →	0.8378, −0.8235, 0.2493, −0.2940	0.7588	39.5	0.285	0.253	58
		Θ's →	0.9586, −0.2340, −0.0112			0.137	0.185	42
241	0.64	Φ's →	1.3840, −0.9879, 0.2196, −0.0621	0.7543	40.0	0.207	0.935	36
		Θ's →	1.2830, −0.2049, −0.1852			0.120	0.231	64

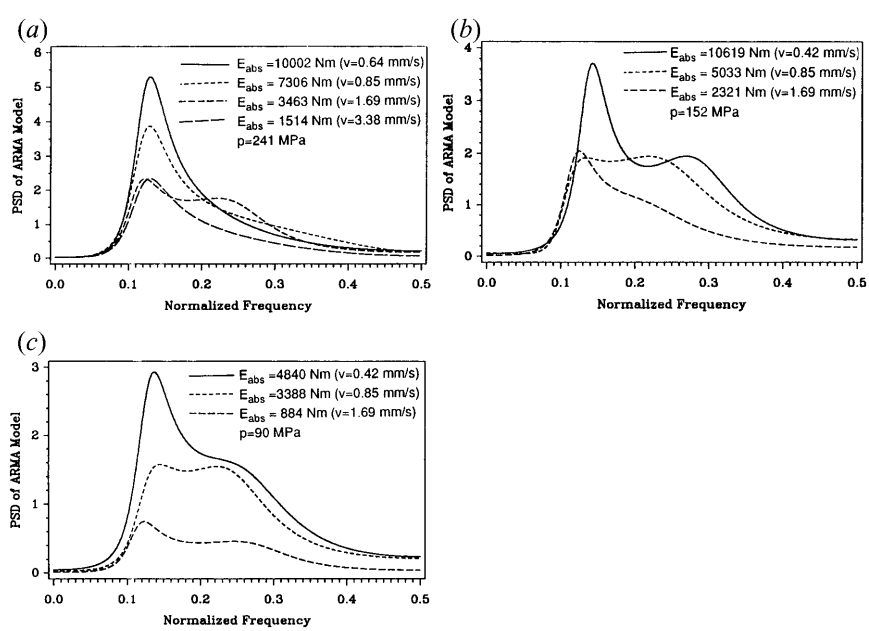

Fig. 8. Plot of PSD-curves for different erosion conditions. (*a*) p = 241 MPa. (*b*) p = 152 MPa. (*c*) p = 90 MPa.

found to be concentrated at around a frequency of 150 kHz (Fig. 8(*a*)). As pressure reduces, the cut becomes shallower and the PSD-peak drops and spreads over a wider frequency range (150–300 kHz). This is illustrated in Figs 8(*b*) to 8(*c*). This trend shown by the AE-signals could be attributed to the change in hydrodynamic effects and the machining mode. From the results of the AE-measurements in fluid-assisted particle erosion [45], it can be assumed that the presence of the rebounded abrasive–water mixture in the narrow kerf region has a damping effect on the AE-signal generated by the material failure processes. This damping effect of the rebounded flow can be expected to be higher for deeper cuts. The investigations of Momber et al. [37] on wear debris removed from grey cast iron by HAM, also indicated that the distribution modulus of the estimated debris size-distribution function decreases as water pressure increases, indicating that the debris particles are of uniform size at high pressure levels. As this indicates a comparatively steady-state material removal process, this could also be a reason for the concentrated frequency response at higher water pressures. Probably, the local energy is high enough to exceed even the highest local resistance energy level in the material, and the material removal process becomes independent of the distribution of the local material properties cited in Eq. (14).

Frequency decomposition of the ARMA-models provides information about the frequencies contributing to the total power of the model and the physical phenomenon responsible for these frequency components. Each ARMA (4,3) model was found to be a combination of two pairs of complex conjugate roots with corresponding damped natural frequencies contributing to the exponentially decaying dynamic mode. The respective damped natural frequency, power and the damping ratio of each complex root are given in Table 4. It can be seen that one root of each model has a damped natural frequency of above 200 kHz, and for the other root it is below 140 kHz. For a given abrasive flowrate of $\dot{m}_P = 0.3$ kg min^{-1}, and abrasive mesh size of 36, the average number of abrasive particles entrained in the mixture is about $\dot{N}_P = 120\,000$ s^{-1}. The damped natural frequency observed below 140 kHz matches quantitatively with the average number of abrasive particles entrained in the mixture.

The root with the higher power can be considered as the primary root, and the root with the lower power is considered as a secondary root. It can be seen from Fig. 8 that for the pump pressures of $p = 90$ MPa and $p = 152$ MPa, the primary frequency for all the roots is observed to be above $f_A = 200$ kHz, whereas for a pump pressure of 241 MPa the primary frequency is about 120 kHz (except in one case). This indicates that at higher pressures ($p = 241$ MPa) the impingement of abrasive particles and resulting material fracture caused by cracking, micromachining, etc. are the primary factors contributing to the power of the AE-signal. The higher damping ratio ($>1/\sqrt{2}$) for the secondary roots of the models at $p = 241$ MPa (see Table 4) is responsible for the absence of the corresponding peak in the PSD-plot, as illustrated in Fig. 8(*a*). Thus, the presence of a larger quantity of water (due to larger flowrate) in the kerf volume at $p = 241$ MPa contributes to the damping of the higher frequency content of the AE-signal. As noted earlier, this high-frequency component is caused by hydrodynamic factors such as turbulence, cavitation, etc.

At $p = 152$ MPa, with an increase in the erosion depth caused by reduced traverse rate (i.e. increased exposure time), the value of the primary frequency increases and its damping ratio reduces (see Table 4). A lower damping ratio indicates a sharper peak response in the PSD-plot. As the primary frequency is observed in the range of $f_A = 215$–285 kHz, it can be concluded that the hydrodynamic effects of the abrasive–water mixture have a stronger influence on the AE-signal than the material removal process. Similar observation can be made for $p = 90$ MPa also as the primary frequency response is in the range of $f_A = 243$–275 kHz.

4.4 Monitoring of Energy Dissipation Using the AE-Technique

AE-signals can be used as an indication of the energy dissipated during HAM. The area enclosed by the PSD-curve, as shown in Fig. 8 and discussed above, can be considered as a quantitative measure of the total energy of the AE-signal for each erosion condition. Figure 9 shows the plot of the calculated dissipated energy versus the measured energy of the AE-signal. The AE-signal energy, E_{AE}, has a relationship ($R^2 = 0.951$, $\sigma = 0.0026$) with the dissipated jet energy given by the following function:

$$E_{AE} \propto \sqrt{(E_{DISS})} \tag{17}$$

This quantitative relationship fits very well into the energy relationships estimated for other machining operations. Matsuoka et al. [16], for example, found experimentally a square-root relationship between the AE_{RMS} and the material removal power for abrasive machining of manganese zinc ferrite. Furthermore, for orthogonal machining, Kannatey-Asibu and Dornfeld [4] analytically developed a relationship between the energy content of AE-signals (AE_{RMS}) and the work rates in the primary and secondary shear zone. The analysis also led

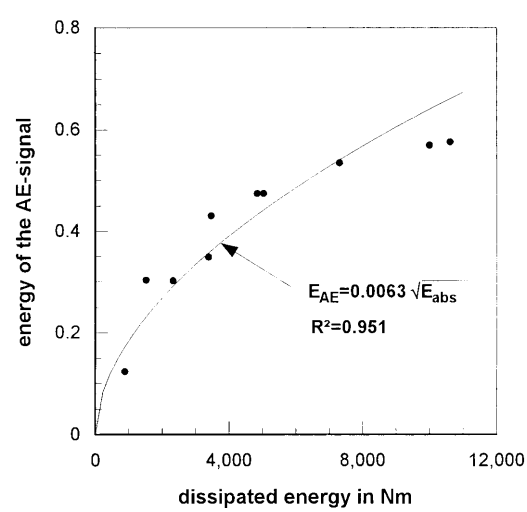

Fig. 9. Relationship between the calculated dissipated energy and the measured energy of the AE-signals.

them to a square root law; it seems that this qualitative agreement points to a certain amount of micromachining during HAM as illustrated by the two pieces chip-like debris shown in Fig. 5.

The experimental points at the lefthand bottom corner of Fig. 9 relate to shallow kerfs, whereas those at the righthand top corner are for deeper cavities. The AE-signal is more responsive to change in dissipated jet energy at shallow kerfs. This trend verifies the previous observations from the frequency characteristics in terms of the increasing damping effect of the rebounded flow for deeper cavities. The input energy dissipated in mechanisms, such as fluid film damping and turbulence, which do not contribute to the material removal, could be another cause for this trend. Thus, the AE-sensing technique can be used effectively to control the dissipated energy in HAM.

This result suggests that it will be possibile to monitor the surface quality of HAM using the AE-sensing technique, as the dissipated energy has already been found to be a possible indication of the surface quality [35].

5. Conclusions

A physical energy dissipation model has been proposed to determine quantitatively the energy dissipated during HAM by different mechanisms, such as plastic deformation, material fracture, wall friction, cavitation, turbulent vortices, damping, etc. The model delivers:

$$E_{DISS} = \frac{\alpha^2 \varphi^2 d_F (\dot{m}_P + \dot{m}_W)}{v\rho_W \left(1 + \frac{\dot{m}_P}{m_W}\right)^2} [p - p_T]$$

The energy dissipated in the workpiece is estimated to be 60%–90% of the input energy for pocket erosion.

The frequency response of the AE-signal is relatively flat beyond a frequency of 500 kHz. AE-signals generated in the workpiece at higher water pressures (p = 241 MPa) were found to be concentrated around f_A = 120 kHz. This frequency matched quantitatively the average number of abrasive particles entrained in the abrasive–water mixture. The presence of uniform debris particles at that pressure causes a concentrated frequency response. The AE-frequency response was found to be at a wider frequency range of 100–300 kHz for lower water pressures which could be due to non-uniform debris particle size and the stronger influence of hydrodynamic effects on the AE-signal.

The power spectrum density of the ARMA-model of the time domain AE-signal is found to be a better parameter than the frequency domain AE-signal for differentiating the various energy dissipation levels. Any parameter change which tends to increase the energy dissipated during machining causes an upward shift in the PSD-curve.

The AE-signal energy given by the area enclosed by the PSD-curve has a square-root relationship (R^2 = 0.951) with the dissipated energy. Hence, it could be used as a parameter to monitor the dissipated energy. This result suggests the possibility of monitoring the HAM-performance (surface quality, erosion depth, surface topography) by the AE-sensing technique in future.

Acknowledgements

The authors are grateful to The University of Tulsa, Tulsa, OK, to the Alexander von Humboldt Foundation, Bonn, Germany, and to the German Research Association, Bonn, Germany, for financial support. Thanks are addressed also to the Center for Robotics and Manufacturing Systems, University of Kentucky, Lexington, KY, for permission to use experimental facility.

References

1. R. H. Sturges, "Monitoring milling processes through AE and tool/part geometry", Transactions ASME Journal of Engineering for Industry, 114, pp. 8–14, 1992.
2. S. M. Pandit and J. D. Stacey, "Data dependent system analysis of acoustic emission in grinding", PED 64, ASME, New York, pp. 437–444, 1993.
3. T. Blum and I. Inasaki, "A study on acoustic emission from the orthogonal cutting process", ASME Journal of Engineering for Industry, 112, pp. 203–211, 1990.
4. E. Kannatey-Asibu and D. Dornfeld, "Quantitative relationships for acoustic emission from orthogonal metal cutting", ASME Journal of Engineering for Industry, 103, pp. 330–340, 1981.
5. R. J. Bones and S. L. McBride, "Adhesive and abrasive wear studies using acoustic emission techniques", Wear, 149, pp. 41–53, 1991.
6. O. Derakhshan, J. R. Houghton, R. K. Jones and P. A. March, "Cavitation monitoring of hydroturbines with RMS acoustic emission measurement", ASTM STP 1077, pp. 305–315, 1991.
7. J. Webster, I. Marinescu and R. Bennett, "Acoustic emission for process control and monitoring of surface integrity during grinding", Annals CIRP, 43, p. 1, 1994.
8. S. L. Jung, K. Prisbrey and G. Wu, "Prediction of rock hardness and drillability using acoustic emission signatures during indentation", International Journal of Rock Mechanics and Mining Sciences, 31, pp. 561–567, 1994.
9. G. Chryssolouris, P. Sheng, N. Anastasia and M. Domroese, "Investigation of acoustic sensing for laser drilling", Transactions of NAMRI/SME, 20, pp. 227–233, 1992.
10. R. Mohan, "Investigation of effects of high-speed coolant on surface grinding performance", PhD thesis, University of Kentucky, Lexington, KY, March, 1996.
11. T. Blum and D. A. Dornfeld, "Grinding process feedback using acoustic emission", MR90–525, Proceedings of the 4th International Grinding Conference of SME, Dearborn, MI, 1990.
12. W. Hundt, D. Leunberger and F. Rehsteiner, "An approach to monitoring of the grinding process using acoustic emission (AE) technique", Annals CIRP, 43, p. 1, 1994.
13. W. Koenig, Y. Altintas and F. Memis, "Direct adaptive control of plunge grinding process using acoustic emission (AE) sensor", International Journal of Machine Tools and Manufacture, 35, pp. 1445–1457, 1995.
14. J. J. Liu and D. A. Dornfeld, "Monitoring of micromachining process using acoustic emission", Transactions of NAMRI/SME, 22, pp. 189–195, 1992.
15. T. Okamura, R. Oshima, K. Satoh and J. Satoh, "Erosion intensity of submerged cavitating jets", in P. Woods (ed.), Proceedings of the 9th International Symposium on Jet Cutting Technology, BHRA Fluid Engineering, Cranfield, pp. 37–48, 1988.
16. K. Matsuoka, D. Forrest and M. K. Tse, "On-line wear monitoring using acoustic emission", Wear, 162, pp. 605–610, 1993.
17. S. Lingard and K. K. Ng, "An investigation of acoustic emission in sliding friction and wear of metals", Wear, 130, pp. 367–379, 1989.

18. S. Lingard, C. W. Yu and C. F. Yau, "Sliding wear studies using acoustic emission", Wear, 162, pp. 597–604, 1993.
19. C. L. Jiaa and D. Dornfeld, "Experimental studies of sliding friction and wear via acoustic emission signal analysis", Wear, 139, pp. 403–424, 1990.
20. F. Guiberteau, N. P. Padture and B. R. Lawn, "Effect of grain size on Hertzian contact damage in alumina", Journal of the American Ceramics Society, 77, pp. 1825–1832, 1994.
21. A. W. Momber, "Concrete failure due to air–water jet impingement", Journal of Materials Science, 35, pp. 2785–2789, 2000.
22. G. S. Choi and G. H. Choi, "Process analysis and monitoring in abrasive water jet machining of alumina ceramics", International Journal of Machine Tools and Manufacture, 37, pp. 295–307, 1997.
23. R. Mohan, A. W. Momber and R. Kovacevic, "On-line monitoring of depth of AWJ penetration using acoustic emission technique", in N. G. Allen (ed) Jet Cutting Technology, Mechanical Engineering Publications, London, pp. 649–664, 1994.
24. A. W. Momber, R. S. Mohan and R. Kovacevic, "On-line analysis of hydro-abrasive erosion of pre-cracked materials by acoustic emission", Theoretical and Applied Fracture Mechanics, 31, pp. 1–17, 1999.
25. A. W. Momber, R. S. Mohan and R. Kovacevic, "An acoustic emission study of cutting bauxite refractory ceramics by abrasive water jets", ASM Journal of Materials Engineering and Performance, 8, pp. 450–454, 1999.
26. R. Kovacevic, H.-S. Kwak and R. Mohan, "Acoustic emission sensing as a tool for understanding the mechanisms of abrasive waterjet drilling of difficult-to-machine materials", Institution of Mechanical Engineers, Journal of Engineering Manufacture, 212, pp. 45–58, 1998.
27. M. Ramulu and D. Arola, "Waterjet and abrasive waterjet cutting of undirected graphite/epoxy composite", Composites, 24, pp. 299–308, 1993.
28. R. Kovacevic, R. Mohan and H. E. Beardsley, "Monitoring of thermal energy distribution in abrasive waterjet cutting using infrared thermography", ASME Journal of Manufacturing Science and Engineering, 118, pp. 555–563, 1996.
29. A. W. Momber and R. Kovacevic, Principles of Abrasive Water Jet Machining, Springer-Verlag, London, 1998.
30. A. W. Momber and R. Kovacevic, "Calculation of exit energy in abrasive water jet cutting", in W. E. Alzheimer (ed.) Manufacturing Science and Engineering, vol. 1, pp. 361–366, ASME, New York, 1994.
31. A. W. Momber and R. Kovacevic, "Quantification of energy absorption capability in abrasive water jet machining", Institution of Mechanical Engineers, Journal of Engineering Manufacture, 209, pp. 491–498, 1995.
32. A. W. Momber and R. Kovacevic, "An energy balance of high-speed abrasive water jet erosion", Institution of Mechanical Engineers, Journal of Engineering Tribology, 213, pp. 463–472, 1999.
33. E. Nadeau, G. D. Stubley and D. J. Burns, "Prediction and role of abrasive velocity in abrasive water jet cutting", International Journal of Water Jet Technology, 1, pp. 109–116, 1991.
34. G. Zhou, M. Leu, E. Geskin, Y. C. Chung and J. Chao, "Investigation of topography of waterjet generated surfaces", PED 62, ASME, New York, pp. 191–202, 1992.
35. S. P. Raju and M. Ramulu, "Predicting hydro-abrasive erosive wear during abrasive waterjet cutting: Part 1", in W. E. Alzheimer (ed.), Manufacturing Science and Engineering, vol. 1, ASME, New York, pp. 339–351, 1994.
36. A. W. Momber, "Energy transfer during the mixing of air and solid particles into a high-speed waterjet", Experimental Thermal and Fluid Science 15, pp. 131–141, 2002.
37. A. W. Momber, H. Kwak and R. Kovacevic, "Investigations in abrasive water jet erosion based on wear particle analysis", ASME Journal of Tribology, 118, pp. 759–766, 1996.
38. S. M. Pandit and S. M. Wu, Time Series and System Analysis with Applications, John Wiley, New York, 1982.
39. J. Chao and E. Geskin, "Experimental study of the striation formation and spectral analysis of the abrasive waterjet generated surfaces", in M. Hashish (ed.), Proceedings of the 7th American Water Jet Conference, WJTA, St Louis, pp. 27–41, 1993.
40. D. K. M. Tan, "A model for the surface finish in abrasive waterjet cutting", in D. Saunders (ed.), Proceedings of the 8th International Symposium on Jet Cutting Technology, BHRA Fluid Engineering, Cranfield, pp. 309–313, 1986.
41. A. W. Momber, H. Kwak and R. Kovacevic, "An alternative method for the evaluation of the abrasive waterjet cutting process in gray cast iron", Journal of Materials Processing Technology, 65, pp. 65–72, 1997.
42. J. Zeng and T. J. Kim, "Development of an abrasive waterjet kerf cutting model for brittle materials", in A. Lichtarowicz (ed.), Jet Cutting Technology, pp. 483–501, Kluwer, Dordrecht, 1992.
43. R. A. Tikhomirov, V. F. Babanin, E. N. Petukhov, I. D. Starikov and V. A. Kovalev, Gidrorezanie Sudostroitel'nykh Materialov, Sudostroenie, Leningrad, 1987.
44. T. H. Chi, Schneiden mit Hochdruckwasserstrahlen. PhD thesis, TU Chemnitz, 1990.
45. W. Hübner, E. Leitel, A. Rolle, J. Lehmann, G. Bülow and H. D. Hopf, "Schallemissionsanalyse erfaßt Feststoffteilchen-Einschläge", Materialprüfung, 34, pp. 13–16, 1992.

Nomenclature

a_1	constant
a_t	white noise
A, B, C	constants
d_F	focusing nozzle diameter
E_A	input kinetic energy
E_{AE}	AE-signal energy
E_{abs}	dissipated energy
E_{EX}	kinetic energy of the exiting flow after erosion
E_{FR}	energy dissipated by wear debris formation
f	normalised frequency
h	erosion depth
m_A	abrasive–water flow mass
$\dot{m}_P$	abrasive mass flowrate
$\dot{m}_W$	water mass flowrate
p	pump pressure
$P(f)$	power spectrum density function
p_T	threshold pump pressure
R_E	erosion resistance
S_P	surface area of the generated wear particle
t_E	exposure time
v	nozzle traverse rate
v_A	abrasive–water flow velocity
v_W	waterjet velocity
Y_t	amplitude of the AE signal
α	mixing efficiency coefficient
φ	orifice momentum transfer coefficient
Φ_i	ARMA parameter
γ_M	material specific energy
γ_{PL}	energy for plastic deformation and toughening
Θ_i	ARMA parameter
ρ_W	fluid medium (water) density
σ_a^2	variance of the white noise